Interfacial design and structure of protein/polymer films on oxidized AlGaN surfaces

2011 J. Phys. D: Appl. Phys. 44 034010

(http://iopscience.iop.org/0022-3727/44/3/034010)

IOP PUBLISHING JOURNAL OF PHYSICS D: APPLIED PHYSICS

J. Phys. D: Appl. Phys. **44** (2011) 034010 (12pp) doi:10.1088/0022-3727/44/3/034010

Interfacial design and structure of protein/polymer films on oxidized AlGaN surfaces

Samit K Gupta[1], Hao-Hsuan Wu[2], Kwang J Kwak[3], Patricia Casal[1], Theodore R Nicholson III[1], Xuejin Wen[2], R Anisha[2], Bharat Bhushan[3], Paul R Berger[2,4], Wu Lu[2], Leonard J Brillson[2,4] and Stephen Craig Lee[1,5,6,7]

[1] Department of Biomedical Engineering, The Ohio State University, Columbus, OH 43210, USA
[2] Department of Electrical and Computer Engineering, The Ohio State University, Columbus, OH 43210, USA
[3] Department of Mechanical Engineering, The Ohio State University, Columbus, OH 43210, USA
[4] Department of Physics, The Ohio State University, Columbus, OH 43210, USA
[5] Department of Chemical and Biomolecular Engineering, The Ohio State University, Columbus, OH 43210, USA
[6] Davis Heart and Lung Research Institute The Ohio State University 473 W. 12th Ave Columbus, OH 43210, USA

E-mail: lee.1996@osu.edu (S C Lee)

Received 24 July 2010, in final form 9 November 2010
Published 22 December 2010
Online at stacks.iop.org/JPhysD/44/034010

Abstract

Protein detection using biologically or immunologically modified field-effect transistors (bio/immunoFETs) depends on the nanoscale structure of the polymer/protein film at sensor interfaces (Bhushan 2010 *Springer Handbook of Nanotechnology* 3rd edn (Heidelberg: Springer); Gupta *et al* 2010 The effect of interface modification on bioFET sensitivity, submitted). AlGaN-based HFETs (heterojunction FETs) are attractive platforms for many protein sensing applications due to their electrical stability in high osmolarity aqueous environments and favourable current drive capabilities. However, interfacial polymer/protein films on AlGaN, though critical to HFET protein sensor function, have not yet been fully characterized. These interfacial films are typically comprised of protein–polymer films, in which analyte-specific receptors are tethered to the sensing surface with a heterobifunctional linker molecule (often a silane molecule). Here we provide insight into the structure and tribology of silane interfaces composed of one of two different silane monomers deposited on oxidized AlGaN, and other metal oxide surfaces. We demonstrate distinct morphologies and wear properties for the interfacial films, attributable to the specific chemistries of the silane monomers used in the films. For each specific silane monomer, film morphologies and wear are broadly consistent on multiple oxide surfaces. Differences in interfacial film morphology also drive improvements in sensitivity of the underlying HFET (coincident with, though not necessarily caused by, differences in interfacial film thickness). We present a testable model of the hypothetical differential interfacial depth distribution of protein analytes on FET sensor interfaces with distinct morphologies. Empirical validation of this model may rationalize the actual behaviour of planar immunoFETs, which has been shown to be contrary to expectations of bio/immunoFET behaviour prevalent in the literature for the last 20 years. Improved interfacial properties of bio/immunoHFETs have improved bio/immunoHFET performance: better understanding of interfaces may lead to mechanistic understanding of FET sensor properties and to clinical translation of the immunoFET platform.

S Online supplementary data available from stacks.iop.org/JPhysD/44/034010/mmedia

1. Introduction

Label-free biosensors are of considerable interest for various clinical and biological applications. Label-free biomolecular sensors detect analyte biomolecules via the intrinsic characteristics of these molecules, rather than by the use of a molecular tag for detection (label). Such sensors directly transduce a biochemical binding event between analyte molecules and analyte-specific receptor molecules on sensor interfaces into an optical, electrical or mechanical signal

[7] Present address: Davis Heart and Lung Research Institute, The Ohio State University 473 W. 12th Ave Columbus, OH 43210, USA.

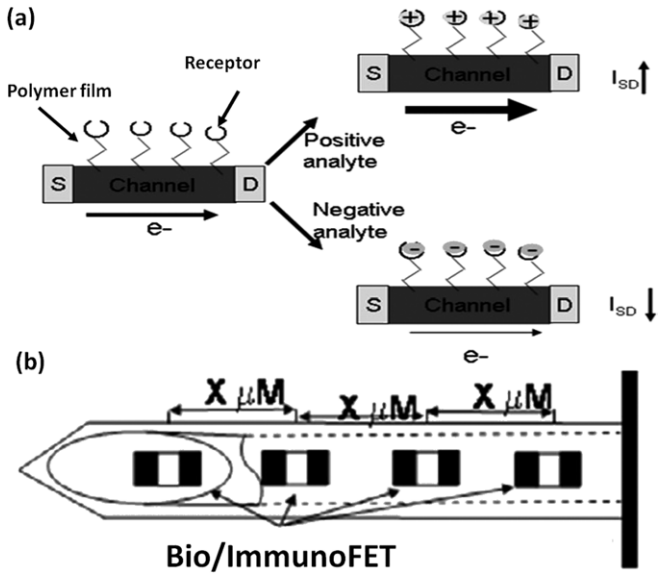

Figure 1. (*a*) Current (I_{SD}) responses of an n-type immunoFET to binding of oppositely charged protein analytes to receptors on the channel. Source (S) and drain (D) contacts are indicated. (*b*) Potential clinical tools for mapping protein concentrations in tissue where individually addressable bio/immunoFETs are mounted on a biopsy needle.

that is detected via the underlying device, and interpreted. Examples include fluorescence resonance energy transfer (FRET) biosensors, silicon-on-insulator, field-effect transistor (FET) biosensors and cantilever sensors (Lud *et al* 2006, Baumgartner *et al* 2009, Bhushan 2010, Estrela *et al* 2010). In these systems, the analyte-specific receptors and the interfaces that contain the receptors critically influence sensor specificity, sensitivity, response kinetics and detection limits (Gupta *et al* 2010). This report focuses on interfaces of FET-based protein biosensors (BioFETs, and analogous immunoFETs: a specific type of bioFET where an antibody molecule acts as the surface receptor), though many of the concepts presented are broadly applicable to other label-free sensors.

Bio/immunoFETs detect protein due to the field effect induced by charges inherent to the analyte molecule. The electric field from the analyte effectively 'gates' the underlying FET by causing either charge carrier accumulation in the device channel (resulting in a current increase) or depleting charge carriers from the device channel (resulting in a current decrease) (see figure 1(*a*)). The specific effect of an analyte depends upon the polarity of both the analyte and semiconductor carrier charges. In protein-detecting bio/immunoFETs, changes in device current can be small relative to total current, due to multiple factors, including the kinetics of receptor–analyte binding and the limited number of charges each analyte–receptor binding event brings proximal to the FET conducting channel surface. Potentially small signals and the need to operate in an aqueous environment mandate the use of low noise, electrically stable FET platforms for protein sensing applications, such as AlGaN/GaN heterojunction FETs (HFETs, Gupta *et al* 2008, Nicholson *et al* 2010). Since electrons are HFET charge carriers, HFETs are n-type devices.

Bio/immunoFET protein detection requires protein analytes possessing detectable electric fields. Protein charge is influenced by multiple factors, including buffer pH. At any given pH, individual proteins have intrinsic net charges (positive, negative, neutral) determined by individual protein amino acid sequence (i.e. by the isoelectric points of constituent amino acids). Charges are statically localized to specific amino acid residues of folded proteins, and, to the extent that proteins have stable three-dimensional structures, protein charges map to specific positions in space. In addition, FET detection of protein electric fields is a function of the nanoscale distance between analyte charge and the FET channel surface (related *in vacuo*, by the inverse square of that distance, and by higher exponential functions in high osmolarity solutions; Israelachvili 1991, Lud *et al* 2006, Nair *et al* 2008). In high osmolarity biological buffers, the critical detection distances (a few nanometres, Bergveld *et al* 1991, 1996, Schoning and Poghossian 2002, Schoning and Poghossian 2006, Gupta *et al* 2008, Nicholson *et al* 2010) are on the order of the diameters of many globular protein molecules. In bio- and immunoFET sensors, proteins are detected when they interact with a receptor (Cui *et al* 2001, Kang *et al* 2005, 2007, Zheng *et al* 2005) that is typically, but not always, another protein molecule. Receptor molecules are usually deployed on FET sensing surfaces on a polymeric film. The interfacial film allows receptors be deployed in a consistent orientation, and with steric freedom to bind analyte. At issue is whether it is possible to build an interface that holds analyte charges within the critical nanometre distance to device active regions required for sensing by the FET (Bergveld *et al* 1991, Schoning and Poghassian 2002, Eteshola *et al* 2008, Gupta *et al* 2008, Nair *et al* 2008, Nicholson *et al* 2010, Wen *et al* 2010).

In toto, the foregoing implies that, providing that proteins analytes have suitable charge distributions and are held stably in controlled orientations relative to sensing channels, differentially charged regions of proteins might be sensed independent of one another by sensors with appropriately designed analyte receptors. The phenomenon has yet to be demonstrated, and bio/immunoFETs are typically thought of as sensing analytes as net charges. Here we discuss interfacial design concepts that impact sensor operating properties, as well as propose interfacial designs that might allow resolution of differentially charged analyte regions.

In addition to analyte–surface proximity and analyte orientation, interfacial wear is also a major consideration in bioFET interface design for *in vivo* applications. Figure 1(*b*) presents a conceptual schematic illustrating a needle-based tissue mapping tool that could be used to determine the distribution of specific proteins with respect to different tissue depths in a given patient. This protein concentration mapping tool is illustrated for the analyte monokine induced by interferon gamma, a protein for which concentration is directly associated with magnitudes of inflammatory states (Ogawa *et al* 2002, Romagnani *et al* 2002, Ruschpler *et al* 2003, Takahata *et al* 2003, Teixeira *et al* 2004). Increasing MIG concentrations are associated with multiple incipient biological processes, including the immune rejection of allografts (Muira *et al* 2001, Reiners *et al* 2002, Zhao *et al* 2002, Fahmy *et al* 2003, Muira *et al* 2003). A MIG

mapping tool would be a powerful research tool in transplant biology, but, perhaps more importantly, could be used for early detection of transplant rejection in patients.

For the tool of figure 1(*b*) to be practical, the polymer–receptor interface of the FET sensors must tolerate (or be protected from) forces acting on the interface during tissue insertion and measurement. Should tissue insertion debride interface from the FETs, sensor biochemical specificity is lost. Debrided protein–polymer constituents could also be potentially toxic and/or immunogenic (Lee *et al* 2001, 2004, 2010, Lee 2010 for protein–polymer immunogenicity).

The trivalent silane 3-aminopropyltriethoxysilane (3-APTES) is commonly used for polymer films construction on FET sensing channels. 3-APTES can produce self-assembled monolayers (SAMs), but when deposited from liquid media, it frequently produces networked interfaces as a result of silane–silane polymerization (Kallury *et al* 1994, Han *et al* 2006, Bhushan *et al* 2009). Polymerization can be avoided using the mono-alkoxy silane aminopropyldimethylethoxysilane (APDMES). Silane polymerization status is potentially important as it influences interfacial thicknesses, and therefore critical analyte-sensing channel distances. Networked 3-APTES interfaces are also less mechanically robust than are APDMES interfaces (Bhushan *et al* 2009).

Multiple attributes make AlGaN/GaN HFETs (heterojunction FETs) amenable to bio/immunoFET use in physiological salt environments, not the least of which is the impermeability of the AlGaN surface to alkaline buffer ions (Kang *et al* 2005, 2007, Gupta *et al* 2008). Here we report partial characterization of AlGaN and chemically similar microfabricated surfaces, by multiple techniques, including angle-resolved x-ray photoelectron spectroscopy (AR-XPS), atomic force microscopy (AFM) and enzyme-linked immunosorbent assay (ELISA). The data presented here shed light on the interfacial structure, and, therefore, electrical behaviour and design features of protein FET sensors.

2. Materials and methods

2.1. Oxidation of AlGaN surfaces

The wafers we used were 23 nm $Al_{0.3}Ga_{0.7}N$ over GaN (Cree Inc., Durham, NC). Before the surface oxidation of AlGaN, the substrates were cleaned by acetone followed by isopropyl alcohol (IPA) in clean room. This chemical treatment is to remove the contaminants on the surface of AlGaN/GaN wafers. AlGaN/GaN wafers were rinsed in deionized water. This step is to remove the chemical residue on the surface of AlGaN/GaN substrates. AlGaN/GaN wafers were placed in an oxygen plasma machine (Anetch asher, PA) and processed under 75 W of power rate and 700 mTorr of pressure. The oxidation time was 30 s.

2.2. Preparation and deposition of 3-APTES and APDMES on plasma-oxidized AlGaN

Oxidized AlGaN chips were boiled in DI water for 30 min to ensure hydroxylation of surface oxides. Subsequently, these chips were baked dry at 70 °C to remove any residual water. For 3-APTES treatment, chips were exposed to a solution of 2% 3-APTES in acetone for 50 min. After treatment, the chips were rinsed three times in acetone and baked for 30 min at 70 °C. For APDMES treatment, chips were exposed to a solution of 5% APDMES in ethanol overnight at 50 °C. After treatment, chips were rinsed once with 1mM acetic acid in ethanol, and twice with ethanol. Chips were baked for 30 min at 70 °C.

2.3. Ellipsometry

The film thickness was measured using an ellipsometer with a nominal thickness resolution of 0.2 nm (Gaertner Scientific LI15CLC waferscan with LI16 microspot optics). A He–Ne laser with a beam wavelength of 632.8 nm was used, with the angles of reflection and incidence set at 708. The polarizer drum was fixed at 458. The laser beam projected on the sample surface produced an elliptical spot size of approximately $30 \times 50\ mm^2$. The uncoated wafer was mounted on the sample stage. By looking through the eyepiece and rotating the X- and Y-plane tilt adjustment controls, sample surface out-of-flatness conditions were corrected. The real (N_s) and extinction values (K_s) of the refractive index of the sample, which is Si with a very thin film of native oxide, were measured; typical measured values for N_s and K_s were 4.00 and 0.30, respectively. For comparison, the refractive index of Si is 3.49 (Lide 2003), and the value for SiO_2 is 1.46 (Shackelford and Alexander 2001). Five measurements at various locations were made by translating the Si-based sample with the aid of a stepper motor. The N_s and K_s (measured previously) and the refractive indices of 3-APTES and APDMES, which are 1.4225 and 1.4276, respectively (Gelest Silanes and Silicones Catalog 4000A, 2008), were entered into the film measurement subprogram in the software. The film thickness was measured using the algorithm provided by the manufacturer.

2.4. X-ray photoelectron spectroscopy (XPS)

XPS is a surface-sensitive technique capable of measuring atomic composition, chemical bonding and depth distribution of elements within the outer few monolayers of a solid. It is based on incident x-rays incident on a solid surface that excite photoelectrons from individual atoms within the solid. A spectrometer collects these photoelectrons and analyses their kinetic energy. The resultant photoelectron intensity versus kinetic energy data comprise an XPS spectrum. The photoelectron's kinetic energy E_K is related to the binding energy E_B of a specific atomic orbital according to the relation $E_K = h\nu - E_B$, where $h\nu$ is the incident photon energy. In turn, the core level energies are characteristic of distinct core levels of specific elements. In addition, shifts of these energies around their characteristic values can indicate 'chemical shifts' due to different chemical environments. The surface sensitivity of XPS is based on the extremely short scattering length of electrons within a solid, typically 2–20 Å depending on their kinetic energy when excited with conventional x-ray sources such as the AlKα source ($h\nu = 1486.6$ eV) used here. Only electrons that emerge from the solid without scattering retain their initial kinetic energy so that only electrons from the outer

few atomic layers contribute useful core level information. Furthermore, the extremely short photoelectron 'escape depth' facilitates XPS measurement of composition and bonding as a function of depth within the outer few monolayers. Here we use the angle-resolved capability of our PHI VersaProbe (Physical Electronics, Inc., Chanhassen, MN, USA) to collect photoelectrons as a function of angle with respect to the overlayer-deposited surface. Photoelectrons collected from the surface at an angle θ relative to the surface plane contribute to the XPS spectrum from depths $d = \lambda \sin \theta$, where $\lambda \simeq 16$ Å is the electron scattering length for the N 1s core level at $E_K = 1089$ eV and the O 1s level at 955 eV. Hence the intensity of the substrate emissions (I_S) decreases from initial intensity I_0 with decreasing analyser collection angle θ according to the Beer–Lambert relationship $I_S = I_0 * e^{-d/(\lambda \sin \theta)}$. Thus at small θ, the XPS spectrum becomes even more surface sensitive.

2.5. Wear testing of interfacial proteins using AFM

Surface morphology, adhesion, friction and wear measurements were made using an AFM (Digital Instruments, Santa Barbara, CA) in air and a liquid environment as described previously in Bhushan *et al* (2009). Briefly, for these studies, square pyramidal Si_3N_4 probes (OTR4-TR; Digital Instruments, Santa Barbara, CA) with a nominal 15–20 nm tip radius mounted on triangular Si_3N_4 cantilevers with a spring constant of 0.08 N mK1 and a resonance frequency of 8–9 kHz were used.

Wear tests were conducted in the contact mode in air and in the tapping mode in liquid environments. For wear tests of silane polymer films in air, a $1 \times 1\,mm^2$ area was scanned at a normal load of 100 nN and then a $3 \times 3\,mm^2$ area was imaged and the average wear depth was calculated. For wear tests in PBS, a $1 \times 1\,mm^2$ area was scanned at a desired normal load and then a $3 \times 3\,mm^2$ area was imaged at minimum possible normal load, to image the wear marks without any distortion. The excitation frequency in the tapping mode used was 8.5 kHz. By adjusting the drive amplitude voltage (voltage supplied to the piezoelectric vibrator), the initial amplitude setpoint was maintained at approximately 1.0 V. The approximate applied normal load in the tapping mode can be obtained by multiplying the amplitude setpoint voltage (V), the conversion factor (50 nm VK1) obtained from the AFM settings and the cantilever stiffness (0.08 nN nmK1). The equivalent calculated normal load for 50% of the free tapping amplitude is 2 nN. Multiple experiments for each test matrix were conducted to verify the trends.

2.6. ELISA quantification of proteins bound to silane films

After silanization with 3-APTES or APDMES, AlGaN wafer fragments (chips) were biotinylated using Sulfo-NHS biotin (Pierce, Rockford, IL), rinsed three times in deionized water and put into individual vials with 330 μl of a 470 nM solution of streptavidin-HRP (SA-HRP, Pierce, Rockford, IL, USA) in phosphate bufferered saline (PBS). Chips were incubated in SA-HRP for 5, 10, 30 and 60 min, then rinsed three times in PBS and transferred to new vials containing 200 μl o-phenylenediamine (OPD) solution prepared as directed by the manufacturer (Sigma, St Louis, MO, USA). After 20 min of incubation, the OPD solution was pipetted into wells of a 96-well ELISA plate containing 50 μl 3M H_2SO_4. The absorbance at 490 nm of each well was measured. The signal was then normalized to the chip surface area (i.e. absorbance unit s/area of chip).

3. Results

3.1. Oxidation of AlGaN surfaces

The AlGaN surfaces of the protein-detecting HFETs were previously oxidized by a wet chemical protocol. Subsequently, a room-temperature oxygen plasma oxidation method was adopted because it induces few defects in the AlGaN surface. Oxidation protocols, and physical/chemical comparison of wet chemical and plasma-oxidized AlGaN surfaces can be found elsewhere (Wen *et al* 2010). The N 1s AR-XPS spectrum of the plasma-oxidized AlGaN is shown in figures 2(*a*) and (*b*), and exhibits 'chemically shifted' contributions from N bonded to O in the oxide, N bonded to Al and Ga in the AlGaN layer, and Ga Auger peaks. The N–O bonding peak is evident only for the $\theta = 10^\circ$ spectrum. The N–AlGa bonding peak increases by nearly an order of magnitude with increasing θ from $\theta = 10^\circ$ to 45°. By contrast, the O 1s spectrum (not shown) exhibits a single peak that increases by only 2.3× with increasing θ, indicating that the O 1s versus N 1s peak intensity ratio I_O/I_N is ∼5× higher at 10° than at 45°. This is consistent with a thin oxide over a N-containing substrate. From the angle dependence and the Beer–Lambert expression (Watts and Wolstenholme 2003), an oxide thickness of 7.5 + 0.3 Å was obtained. For the plasma oxidation conditions used, this thickness is consistent with an average 6 Å surface oxide reported for a 30 s, 50 W oxygen plasma and a 12 Å thick oxide for a 480 s exposure. Furthermore, Ga 3d and Al 2p core level spectra show a nearly 3 : 1 Ga : Al composition ratio in the oxynitride, increasing to 4 : 1 at the oxynitride–vacuum interface, whose composition is 8.3% Al, 20.5% Ga, 17.7% O, 12.7% C and 40.7% N. This implies that while oxidized, sputter-coated Al may be an economical model of chemically oxidized AlGaN surfaces (as in Bhushan *et al* (2009)), it may be less appropriate to model plasma-oxidized surfaces due to the significantly higher amounts of Ga oxides found in the surface oxide in comparison with Al oxides (table 1).

3.2. Thickness and wear of interfaces on surfaces mimicking AlGaN oxides

Initial surface analysis was performed on AlGaN analogues (silica and alumina), in part because of the extreme expense of AlGaN material. Various surface properties of APDMES and 3-APTES polymer films were compared on both silica and alumina substrates. As shown in figure 3, the APDMES films were thinner than the 3-APTES films on both the silica and alumina surfaces. AFM data also indicate that 3-APTES films are rougher than the APDMES interfaces on silica (similar trends are seen on alumina surfaces, but the error bars overlap). The APDMES film was more than twofold

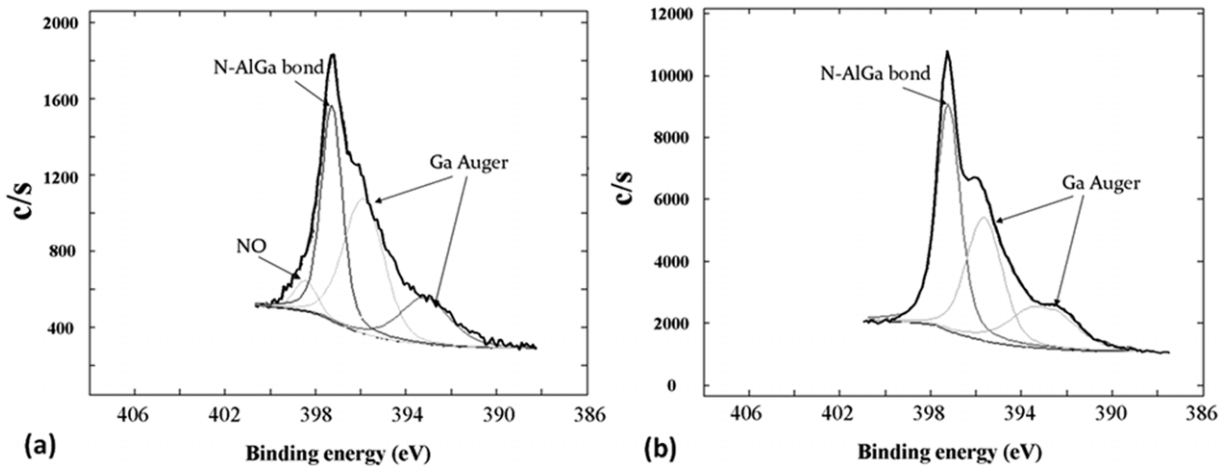

Figure 2. N 1s spectra of an oxidized AlGaN surface at 10° (*a*) and 45° (*b*).

Table 1. Table summarizing angle-resolved XPS study of oxidized AlGaN surface.

XPS analysing angle	Al 2p (%)	Ga 3d (%)	O 1s (%)	C 1s (%)	N 1s (%)
10°	8.27	20.53	17.73	12.73	40.74
20°	8.66	24.53	15.03	7.46	44.37
45°	10.30	31.22	9.34	4.76	44.38

thinner on both silica and alumina, with the ∼1 nm thickness found on both surfaces approximating the summed bond length of a single APDMES monomer (summing bond lengths, alkoxy to amine, ∼1.0 nm), suggesting that the APDMES interface approximates a monolayer. On the other hand, due to the greater thickness and roughness of 3-APTES films, it is likely that the films form a more complex, networked structure that is thicker and more irregular than a monolayer. Further investigation of the interfacial films supported these hypotheses (see below, and Bhushan *et al* (2009)).

Adhesion and coefficient of friction are low for streptavidin functionalized silane films on both silica and alumina. This is as expected, given the well-known lubricating properties of proteins (Liao *et al* 1999, Scholes *et al* 2000, Wang *et al* 2004, Bhushan *et al* 2006), and may reflect the fact that after streptavidin is bound to these interfacial polymer films, the lubricating properties of streptavidin dominate the adhesion and friction properties of the surface (Bhushan *et al* 2005, 2006, Lee *et al* 2005, Shapiro *et al* 2007). These results led to a model of APDMES and 3-APTES interfaces (Bhushan *et al* 2009, figure 1) that is considered in detail, and is extended, in section 4.

Wear properties of APDMES and 3-APTES films on silica and alumina interfaces are compared in figures 4(*a*) and (*b*). The AFM tip was rastered across the surface in the shape of a square under controlled loads (see section 2). APDMES films were more wear resistant than were 3-APTES films, as is apparent in the relative quantities of each interface that were removed by tips at the same loads. Differential mechanical robustness was not only apparent for APDMES and 3-APTES interfaces but also for biotinylated silane interfaces with streptavidin bound to the interfacial biotin.

The differential wear properties of our 3-APTES and APDMES interfaces reflect their distinct structures, as captured in our model (Bhushan *et al* 2009, below). Due to its polymerized architecture, the networked 3-APTES film is likely bonded to the substrate surface by fewer silane monomer–surface oxide bonds per 3-APTES monomer than occur in APDMES films (necessarily, one siloxane linkage to the oxide surface per APDMES monomer). 3-APTES monomers can have as few as zero and a maximum of two siloxane bonds to alumina and silica substrate oxides, if the monomer in question is part of a polymerized 3-APTES structure. Since 3-APTES films are greater than twice the thickness predicted by summed 3-APTES monomer bond lengths, most of a film's constituent individual silane monomers are likely directly bonded to the surface oxide by fewer than one siloxane bond each. 3-APTES films are also internally crosslinked, but APDMES films are not. Furthermore, 3-APTES films are thicker, and therefore have greater opportunity to interact with AFM tips impinging on the film than do APDMES films. These unique structural characteristics of our 3-APTES films are absent from our APDMES films, accounting for the higher vulnerability to mechanical insult exhibited by these 3-APTES-based interfaces. Even after biotinylation and attachment of streptavidin to the interface, the interfacial films exhibited similar trends in terms of wear, lending further support to the argument that differential wear properties are caused by the underlying silane molecules.

3.3. Protein binding behaviour and interfacial structure

3-APTES and APDMES-functionalized surfaces have distinct mechanical properties (thickness, roughness and wear resistance, figures 3 and 4, and Bhushan *et al* 2009). 3-APTES and APDMES films also have distinct biochemical properties, which, like their distinct mechanical properties, can be attributed to their respective structures. During sensor operation, these properties can be expected to influence protein binding behaviour and, therefore, device behaviour.

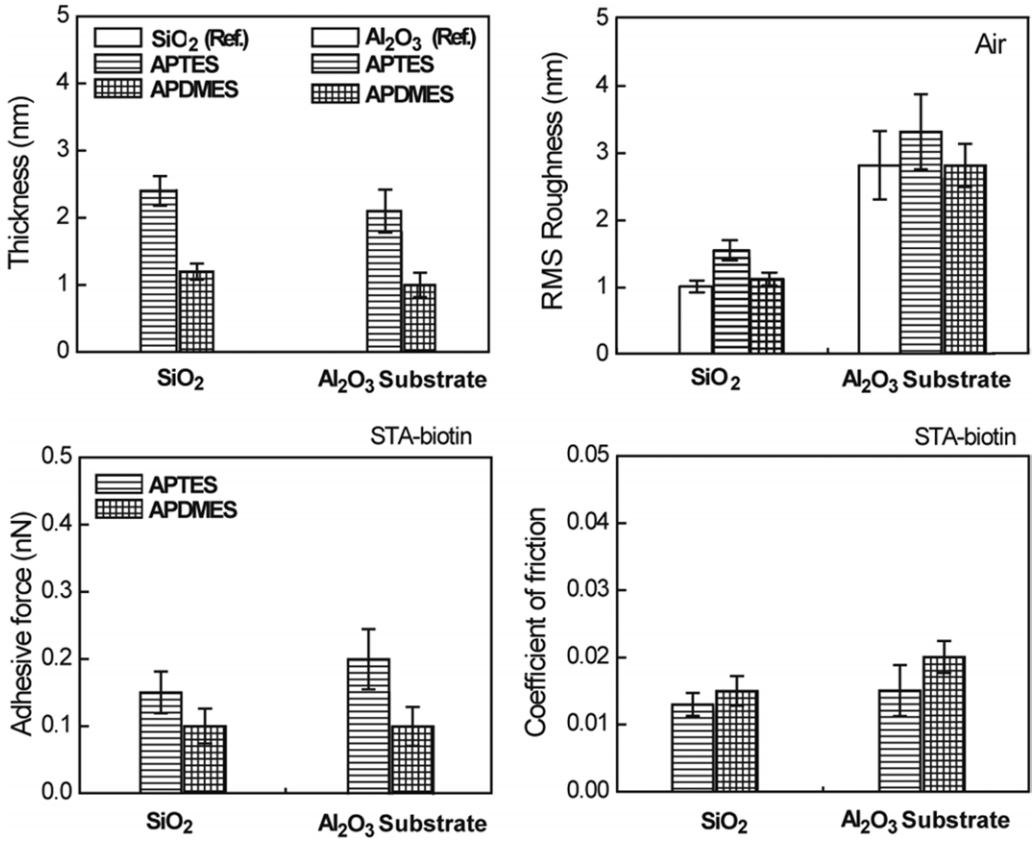

Figure 3. Summary of the film thickness of bare SiO_2 (ref) and Al_2O_3 (ref) and various silane polymer films and adhesive force and coefficient of friction of STA-biotin on various silane polymer films, all in PBS buffer solution. The error bars represent $\pm 1\sigma$.

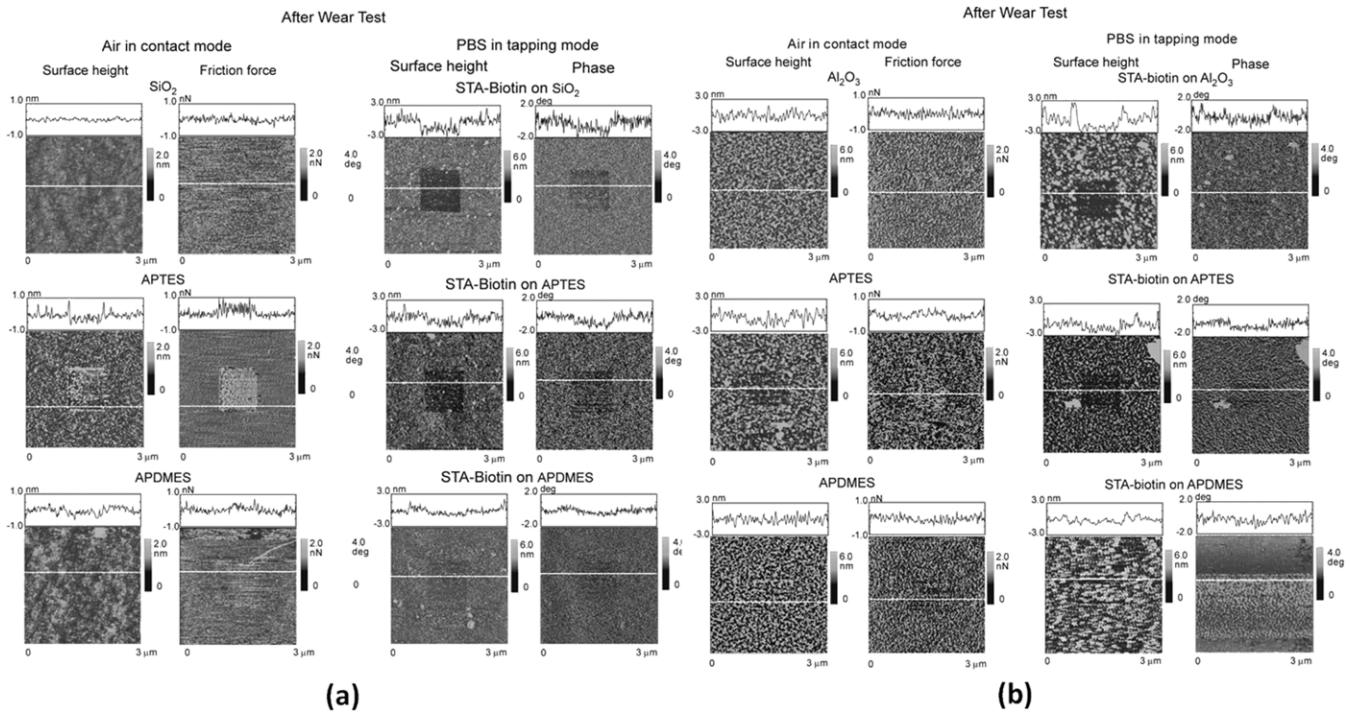

Figure 4. AFM surface height, friction force images and cross-sectional profiles obtained after wear test in air in contact mode at 100 nN on bare substrates and various silane polymer films and PBS in tapping mode for STA-Biotin on bare substrates and various silane films: (*a*) SiO_2 and (*b*) on Al_2O_3 substrates. The white lines indicate the locations for the cross sections.

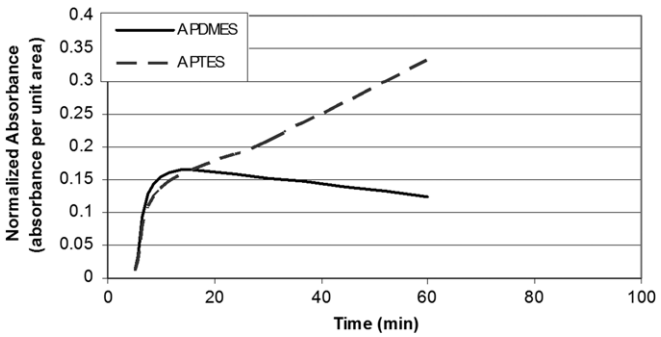

Figure 5. Chip ELISA illustrating difference in binding kinetics to biotinylated silane interfaces. Absorbance value was read at 450 nm, and normalized to chip unit area (mm^2).

It was previously hypothesized that streptavidin binding to 3-APTES films should exhibit diffusion-limited behaviour because the streptavidin molecules must diffuse through the porous 3-APTES structure to reach binding sites within the networked biotinylated 3-APTES film (Gupta *et al* 2008). On the other hand, since APDMES films approximate monolayers, streptavidin binding to biotinylated APDMES interfaces will not exhibit similar diffusion limitations: biotins occur at the surface of biotinylated APDMES films (dictated by the location of amine groups, shown by AR-XPS), but in 3-APTES films, biotins are distributed throughout, as are the terminal amines (see AR-XPS data, below). The hypothesis regarding 3-APTES film structure of Gupta *et al* implies that biochemical saturation of streptavidin binding should occur rapidly for planar films (such as APDMES), but over an extended period of time for biotinylated networked films (such as 3-APTES). This was tested by an ELISA (enzyme-linked immunosorbant assay) time course experiment.

APDMES or 3-APTES silanized AlGaN wafer fragments were biotinylated as described, then exposed to streptavidin-HRP (horse radish peroxidase) protein bioconjugates. HRP bioactivity is detected in ELISA using a chromogenic enzyme substrate (section 2). ELISA signals were measured at varying times following exposure to streptavidin-HRP to establish the binding time course supported by each silane interface. The results are shown in figure 5.

3-APTES-functionalized (wafer 1) and APDMES-functionalized AlGaN wafers (wafer 2) exhibit very different behaviour in the ELISA experiment. Wafer 1 exhibits a biphasic binding curve, with a rapid increase in signal at early time points, followed by a second, linear phase of ELISA signal accumulation. Wafer 2 does not exhibit the same behaviour. The APDMES interface accumulates ELISA signal rapidly to the point of biotin saturation by streptavidin, after which no appreciable increase in the amount of streptavidin bound to the interfacial film is detected. We interpret the data to indicate that streptavidin binding follows rapid kinetics initially as the streptavidin quickly binds the surface-accessible biotins of both the APDMES and 3-APTES interfaces. For the APDMES interface, this rapid kinetics continues until the surface is saturated with stretpavidin binding. However, for the 3-APTES interface, saturation is not achieved, as evidenced by the linear phase of the curve, indicating gradual increase in streptavidin binding to the interface. This supports the previously published hypothesis that streptavidin binding to an 3-APTES interface was diffusion-limited in that for biochemical saturation to occur streptavidin must diffuse into the 3-APTES interface and binds biotins deployed deeper in the 3-APTES film. The APDMES film has no biotins beneath the surface of the film, so signal accumulation stops after the APDMES surface is packed with streptavidin.

Table 2. Ratios of angle-resolved XPS signals at $\theta = 10^\circ$. The ratios indicate the preferential orientation of N versus O, N versus Si and Si versus O.

	N 1s/O 1s	N 1s/Si 2p	Si 2p /O 1s
APDMES	1.10	3.65	0.301
APTES	0.77	2.05	0.375

3.4. 3-APTES and APDMES orientation on AlGaN

AR-XPS measurements of 3-APTES and APDMES at $\theta = 10^\circ$ provide compositions with the highest surface sensitivity whose relative concentrations provide significant information about silane film orientation. Table 2 presents data from the $\theta = 10^\circ$ AR-XPS results for the ratios percentage compositions of each element within the stacked silane film-oxide-AlGaN/GaN surface layers. The full table of percentage compositions can be found in the supplementary data section (stacks.iop.org/JPhysD/44/034010/mmedia). If the structure of 3-APTES films is similar to the model presented in figure 5 (Bhushan *et al* 2009), APDMES should exhibit a stronger preferential orientation of the amine group above the Si and O, and orientation of Si above O, than does 3-APTES, and we expect to observe higher I_{N1s}/I_{Si2p} and I_{N1s}/I_{O1s} ratios in APDMES while I_{Si2p}/I_{O1s} ratios should be more comparable. Upon completion of our AR-XPS study, we found that this indeed was the case (see table 2). The higher I_{N1s}/I_{Si2p}, I_{N1s}/I_{O1s} and $I_{Si2p/O1s}$ ratios confirm the expected strong preferential orientation of the amine group above Si and O in APDMES films.

The data of this paper, taken together, indicate that the model film structures proposed in Bhushan *et al* (2009) and Arranz *et al* (2008) are accurate to the extent that APDMES films are thinner, more mechanically robust, and more strongly oriented siloxane to terminal amine (from the AlGaN surface outwards) than are 3-APTES films (Kallury *et al* 1994, Bhushan *et al* 2005, 2006, 2009, Shapiro *et al* 2007, Arranz *et al* 2008, Gupta *et al* 2008). AFM and ellipsometry data (figure 3) show that 3-APTES films are thicker and rougher on silica than are APDMES films (similar trends are seen on alumina surfaces, though the error bars overlap). Necessarily, a smaller fraction of monomers in a networked structure can be bonded directly to the AlGaN surface (i.e. fewer siloxane bonds per 3-APTES monomer than APDMES films). This likely accounts for wear data of figure 4 showing that 3-APTES films are more fragile (that is, more easily abraded from the surface, Bhushan *et al* 2009) than are APDMES films (Arranz *et al* 2008, Bhushan *et al* 2009). Networked 3-APTES and planar APDMES film structures, respectively, are congruent with

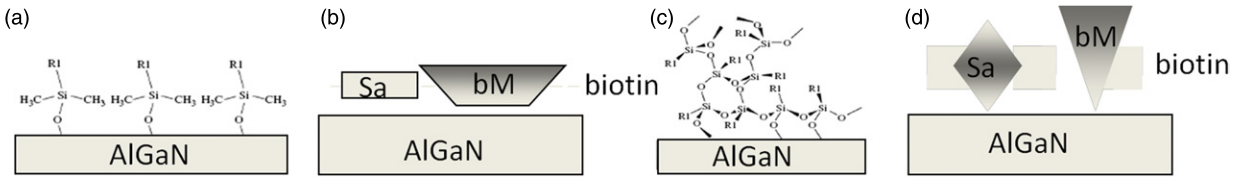

Figure 6. Schematic depictions of silane–protein interfaces on AlGaN surfaces. (*a*) A biotinylated APDMES polymeric film; (*b*) A hypothetical vertical depth-concentration profile of streptavidin and biotinylated MIG on a biotinylated APDMES film; (*c*) A biotinylated 3-APTES polymeric film and (*d*) A hypothetical vertical depth-concentration profile of streptavidin and biotinylated MIG on a biotinylated 3-APTES film. R1 is $CH_2CH_2CH_2NH$–biotin. The hypothetical distribution of biotin in each film is indicated by the grey dashed line (labelled 'biotin'), where the thickness of the line represents the hypothetical distribution of biotin in the silane film. The interfacial polymer film is expected to terminate at the edge of the dashed line farthest from the AlGaN. Hypothetical distribution of streptavdin is indicated by a rectangle or diamond marked 'Sa' and hypothetical distribution of biotinylated MIG is indicated by the shape marked with 'bM'. Expected concentrations of each protein are indicated redundantly by both shading and shape. Areas of anticipated high concentration are indicated by darker, wider areas of the shapes and areas of anticipated lower concentration are indicated by lighter, narrower regions of the shapes. Shading and width representation of protein concentration are meant to be interpreted in the context of a single shape. They are not meant to indicate relative concentrations of different proteins in the same or different polymer films, nor are the shapes and shading intended to indicate the relative concentrations of the same proteins in different polymer films.

ELISA data (figure 5), which reflects the greater diffusional barrier to streptavidin binding posed by 3-APTES films. The proposed film structure for 3-APTES is also congruent with streptavidin-mediated sensor signal accumulation seen in Gupta *et al* (2008), which shows streptavidin signal increasing over time, again reflecting a diffusional barrier to streptavidin binding posed by the networked (3-APTES) film. Finally, the AR-XPS data of table 2 clearly demonstrate that the APDMES films are more preferentially oriented with amine groups localized to the external interfacial surface than in 3-APTES films. Thus, the proposed networked structure of 3-APTES explains biochemical, physical and mechanical properties of the 3-APTES and APDMES films, and corroborates the findings of other investigators (Kallury *et al* 1994, Arranz *et al* 2008).

These differences in the film structure have a profound impact upon biomolecule binding to the interface, and subsequently sensor interface structure and function (seen in Gupta *et al* (2008)). The established differential morphologies of 3-APTES and APDMES films must also influence the distribution of analyte molecules bound to them. Figure 6 shows the distribution of analyte molecules that we expect from the established film structures of 3-APTES and APDMES, and are discussed below.

4. Discussion and concluding remarks

3-APTES and APDMES are frequently used as linker molecules on metal oxide surfaces of microfabricated devices, including sensors, to link receptor molecules to, and orient the receptors on, the surface (Eteshola *et al* 2008, Shapiro *et al* 2007, Nicholson *et al* 2010). The linker layer constitutes an interfacial polymeric film. Understanding film structure and properties is critical to understanding sensor behaviour.

3-APTES molecules can form networked interfaces on metal oxides as a result of the molecules' tri-alkoxy group (Bhushan *et al* 2005, 2006, 2009, Lee *et al* 2005, Arranz *et al* 2008). Both mono- and multilayered 3-APTES films have been reported on oxidized GaN surfaces (Baur *et al* 2005, Arranz *et al* 2008). Interestingly, oxidized p-type and n-type GaN are reported to have different hydroxylation states, leading to distinct morphologies of 3-APTES films on those surfaces (Arranz *et al* 2008). n-type GaN surfaces support formation of networked 3-APTES interfaces, whereas 3-APTES on p-type GaN forms interfaces with monolayer-like morphology.

We build n-type HFETs from AlGaN/GaN heterojunction material that is arguably chemically and electrically similar to n-type GaN, and our data suggest that solution-deposited 3-APTES forms a networked structure on the oxidized AlGaN surface (table 2, Nicholson *et al* 2010, Wu *et al* 2010). Ellipsometry of 3-APTES and APDMES on silica and alumina surfaces (analogues of the AlGaN surface, Bhushan *et al* 2009, figures 3 and 4) revealed 3-APTES films to be substantially thicker than APDMES films. AFM characterization of 3-APTES films on those substrates indicates them to be rougher than APDMES films (Bhushan *et al* 2009, figure 3(*b*)). AR-XPS of silanes deposited on oxidized AlGaN shows that APDMES is more strongly oriented (siloxane group to terminal amine) from the AlGaN surface than is 3-APTES (Wen *et al* 2010, Wu *et al* 2010). 3-APTES layers on multiple substrates (alumina, silica, oxidized AlGaN) thus seem to have a morphology much as described for 3-APTES films on n-type GaN by Arranz *et al* (2008).

We and Arranz *et al* arrived at remarkably similar models of networked 3-APTES on metal oxide surfaces (compare figure 2(*b*) of Bhushan *et al* (2009), to figure 5(*b*) of Arranz *et al* (2008)) at approximately the same time (they were a few months earlier) from different supporting data. Their model follows primarily from AR-XPS data (Arranz *et al* 2008), while ours was supported by a combination of AFM and ellipsometry data (Bhushan *et al* 2005, 2006, 2009, Lee 2005). We have now extended our finding of networked 3-APTES films to AlGaN surfaces with AR-XPS (table 2).

Returning to silane linker films on GaN, Arranz *et al* (2008) argue that the electrical characteristics of the underlying GaN substrate (p- or n-type) make the n-type oxidized surface more amenable to some chemical modifications (hydroxylation of GaN oxides, Arranz *et al* 2008). Differential GaN oxide hydroxylation is thought to drive formation of either 3-APTES monolayers (p-type) or networks (n-type). Arranz *et al* (2008) report similar AFM roughness parameters for the

GaN surfaces, but n-type GaN has been reported elsewhere to be substantially rougher than p-type (Youtsey *et al* 1997), so we cannot completely rule out that the n-type GaN may be more chemically reactive partially as a result of greater surface asperities (i.e. differential surface energy) on the n-type GaN (Arranz 2008). That said, the alumina substrate we used in our AFM studies is substantially rougher than is the silica substrate. Although all 3-APTES and APDMES films we examined were very different from each other in consistent and systematic ways, we detected similar trends in comparing interfacial films made with the same silane compound on different substrates. Nonetheless, recent AlGaN/GaN HFET sensor data suggest that differences in interfacial polymer film morphology significantly influence bio/immunoFET sensitivity (multiple orders of magnitude, Nicholson *et al* 2010, Gupta *et al* 2010).

We initially chose alumina as an inexpensive model for AlGaN, assuming that that aluminium oxide was the most common oxide in the AlGaN surface (Bhushan 2009). We now know that aluminium oxide is only the most prevalent oxide when some (reactive ion etching (RIE) using oxygen plasma), but not other (wet chemical oxidation and ICP or inductively coupled plasma oxidation with an oxygen plasma) oxidation protocols are used (Nicholson *et al* 2010, Wen *et al* 2010). The alumina surface thus turns out not to be a high fidelity model for AlGaN oxides produced by many procedures, including those we use to make HFETs (wet chemical and ICP oxidation, Gupta *et al* 2008, Wen *et al* 2010). However, because AlGaN HFETs may be too expensive for human clinical use, we have experimented with atomic layer deposition (ALD) to deploy high-K, alkaline ion 'impermeable' dielectrics on cheaper FET architectures. Al oxide layers are promising: C–V profiling shows that Al oxide can resist ion permeation after prolonged exposure to high osmolarity buffer (Nicholson *et al* 2010). Bio/immunoFET sensors based on a more economical FET architecture with an aluminium oxide surface may be as feasible in high osmolarity environments as AlGaN HFETs. Surface studies on alumina are thus not only applicable to AlGaN HFETs oxidized via RIE, but also to alumina surfaced bio/immunoFETs.

Differential morphologies of our 3-APTES and APDMES films on AlGaN are reflected in the differential mechanical and chemical properties, as well as differential protein binding kinetics of biotinylated interfaces based on those silanes (figures 3–5, table 2). Based on the suite of data presented here, APDMES interfaces appear to be effectively 'planar', with biotins presented at a more or less consistent distance from the sensor surface, resulting in rapid binding of streptavidin to surface biotins. Streptavidin binding plateaus when surfaces are either biochemically saturated or further streptavidin binding is sterically inhibited. On the other hand, 3-APTES interfaces appear to be complex, networked films with a porous structure (the data presented here lend credence to the hypothesis proposed in Gupta *et al* (2008)): streptavidin rapidly binds the most surface-accessible biotins, but additional streptavidin binding continues at a lower rate as molecules penetrate the 'pores' of the 3-APTES films. At points beyond the initial phase of rapid streptavidin binding, ELISA and fluorescence microscopy both show that more streptavidin binds the 3-APTES interface than the APDMES interface (figure 5 and supplementary data (stacks.iop.org/JPhysD/44/034010/mmedia)).

APDMES interfaces allow detection of lower solution concentrations of protein analytes than do 3-APTES interfaces (Nicholson *et al* 2010, Gupta *et al* 2010). Differential protein binding kinetics seem to suggest that sensors with APDMES interfaces will reach maximum signal more rapidly than do sensors with 3-APTES interfaces. In fact, sensing results with HFETs with 3-APTES and APDMES interfaces should emulate ELISA binding behaviour under similar biochemical conditions, but we cannot test this hypothesis with our current apparatus. A closed, microfluidic analyte delivery system would inhibit sample evaporation and allow us to determine whether sensor signal accumulation recapitulates protein binding behaviour revealed by ELISA. It may not. The greater sensitivity of devices with APDMES rather than 3-APTES interfaces, despite the fact that 3-APTES films can support more analyte binding under some conditions, may be indicative that the average amount of sensor signal accumulated per individual streptavidin binding event may be less on 3-APTES films, and may not be constant over a prolonged time course of streptavidin binding.

The results presented here and elsewhere (Bhushan *et al* 2009, Gupta *et al* 2010, Nicholson *et al* 2010) underscore the importance of the silane–protein interface on FET protein sensor function. Despite the fundamental importance of interfacial structure in bio/immunoFETs, this is an oft-ignored topic in the field (as is pointed out by Bergveld *et al* (2003)). In fact, many reports assume monolayer interfacial structure and coverage by silane–protein films without providing analysis of the interface to verify the claim (Bergveld *et al* 1991, 1996, 2003, Schoning and Poghossian 2002, Kang *et al* 2005, 2007). The suite of data presented here and elsewhere (Kallury *et al* 1994, Arranz *et al* 2008, Gupta *et al* 2008, Bhushan *et al* 2009, Nicholson *et al* 2010, Wen *et al* 2010) drives logical models of analyte binding/distribution on planar and networked interfacial films on FET sensors (figure 6). The analyte distribution model of figure 6 represents a logical extension of interfacial structures that are supported by the data discussed above: figure 6 is based on expected and observed analyte binding behaviour to interfaces with either planar or network morphologies (Kallury *et al* 1994, Arranz *et al* 2008, Gupta *et al* 2008, Bhushan *et al* 2009, Nicholson *et al* 2010, Wen *et al* 2010, Wu *et al* 2010).

Based on our interfacial structural model (Bhushan *et al* 2009), and the differential protein binding behaviour of 3-APTES and APDMES films on AlGaN, we hypothesize that the 3-APTES and APDMES films may support different distributions of receptor and analyte in the interface at biochemical equilibrium, driven by the distinct morphology of the silane films on AlGaN (figure 6). Figure 6(*b*) and (*d*) show the hypothesized distributions of the protein components of the interface once the silanized surface has been treated with NHS-biotin, streptavidin, and then biotinylated MIG. In considering the discussion, it is useful to remember that polymeric and protein components are not rigid, and have some conformational freedom.

NHS-biotin reacts with the interfacial amines of silane films. Streptavidin–biotin interactions have nearly covalent levels of affinity, and streptavidin is typically a tetramer (four biotin binding pockets tetramer) so streptavidin bound to biotinylated interfacial films can also bind to biotinylated analytes (Weber *et al* 1989). In figure 6(*b*), due to the near monolayer structure of APDMES films, biotin (dashed line) is at nearly constant height off the sensing surface. We use shaded geometric shapes to represent the vertical distribution of proteins in the silane films, and darker regions and wider regions redundantly indicate higher protein concentration.

Streptavidin bound to biotinylated APDMES would also reside at a more or less fixed distance from the sensing surface. Because we expect streptavidin to be deployed in a discrete layer in/on the biotinylated silane film without significant variation in its concentration with depth, we represent its depth profile on APDMES with a rectangle. Depending on bound streptavidin orientation, rigidity of interfacial film components and density of the biotinylated APDMES film, we anticipate that biotinylated MIG (b-MIG) concentration will be greatest at or above the streptavidin layer, and decrease moving towards the AlGaN surface. Since we cannot rule out that there may be a decreasing gradient of b-MIG moving deeper into the film, we represent b-MIG's depth profile on APDMES as a trapezoid. For a given APDMES film, how sharply b-MIG's concentration falls off approaching the AlGaN surface should be a function of b-MIG's Stokes radius and its multimerization state (the multimerization state of MIG across its concentration range is debated (Wang *et al* 2003)) in comparison with APDMES film density. Smaller diameter analytes might penetrate the film somewhat more deeply, but presumably any analyte's maximal depth of deployment in the interfacial film is limited by its size and the position/orientation of deployment of streptavidin. We hypothesize a different pattern of deployment of proteins in networked 3-APTES films (figure 6(*d*)).

In the case of 3-APTES-based films, amine groups are distributed throughout much of the film, and subsequent biotinylation of these amines will be influenced by their distribution and the diffusional properties of the biotinylating reagent used. The range of distribution of distances (biotin to AlGaN) is expected to be wider for the networked 3-APTES than for APDMES interfaces (indicated by the thicker dashed line in figure 6(*d*)). The surface of the 3-APTES film may not be composed entirely of amines: AR-XPS shows it to have considerably more carbon (from the propyl group of 3-APTES) than does the APDMES film. Biotin can be appended only to amines, so perhaps unlike the APDMES film there may be a gradient of increasing streptavidin content moving from the outer edge of the interface towards the AlGaN. After prolonged exposure to streptavidin (nearing binding equilibrium), concentration of streptavidin in the film should fall off moving towards the AlGaN surface, but we hypothesize it should fall off less sharply than in APDMES films, because the biotin layer is less discrete in 3-APTES than in APDMES films and 3-APTES films are thicker than APDMES films. The streptavidin depth profile should reflect the relative Stokes radius of streptavidin and the 3-APTES film porosity. The streptavidin depth profile is represented as a diamond to represent these considerations, though the slopes of the sides of the diamond above and below the region of maximal streptavidin concentration may not be identical. We hypothesize that b-MIG concentration will be maximal on the outermost surface, and that concentration will fall approaching the AlGaN surface because its receptor's (streptavidin) concentration falls approaching the AlGaN, and because the porous structure of the 3-APTES film and the presence of space-filling streptavidin-biotinylated MIG complexes impede diffusion of biotinylated MIG to deeper regions of the 3-APTES film. Hence, we represent the biotinylated MIG concentration profile as a triangle.

These suppositions, while not directly supported by data beyond the data driving the APDMES and 3-APTES film structure models and the differential protein binding behaviour of the two silane films, are a logical extension of these (and other) findings. The models of figure 6 are relevant because the deployment of analytes in sensor interfacial films should drive sensor behaviour, and it should be possible to cross-correlate interfacial structure with sensing data. Much as a closed microfluidic analyte delivery system should allow us to determine under what conditions sensor signal accumulation approximates protein binding kinetics, knowledge of the interfacial depth profile correlated with sensing signals will help us determine which interfacial parameters drive signal intensity. We believe that this knowledge will lead us to a model that can account for sensor behaviour, and help design better bio/immunoFETs. More to the point, this discussion is necessary and productive for the bio/immunoFET community, given the lack of attention that has been paid to the importance of interfacial engineering on device function thus far.

Another corollary of the differential structures of 3-APTES and APDMES films is differential mechanical robustness of the two films. On silica and alumina substrates, APDMES films are more robust. As shown in figure 6, in APDMES interfaces each APDMES molecule is attached to the oxidized AlGaN surface via a siloxane bond, whereas in 3-APTES interfaces, the entire networked polymeric film is attached by only a few siloxane bonds. Hence, force applied to one monomer in the 3-APTES interface can be transferred to the entire 3-APTES film, but this is not the case in APDMES films, wherein force applied to individual monomers cannot be transferred to other monomers in the film through monomer–monomer covalent bonds. Application of force to one portion of the 3-APTES layer can pull the entire film back, much in the way one pulls back a sheet on a bed.

There may be similar wear differences between 3-APTES and APDMES films on AlGaN, as well as between films of the same silanes deposited on differentially oxidized AlGaN surfaces (Wen *et al* 2010), at least to the extent that 3-APTES and APDMES films on AlGaN are similar to corresponding films on alumina and silica. The magnitude of tribological differences between 3-APTES and APDMES films on AlGaN are under investigation as interfacial film robustness is critical to sensor function. If the receptor layer debrides from the bio/immunoFET surface, the device retains sensitivity to charge, but loses specificity for analyte binding. If a MIG FET sensor is deployed on a needle for insertion into

grafts (as in figure 1(*b*)), abrasive insult to the interfacial film could come from insertion of the needle probe into tissue or operator or patient movement. Furthermore, polymer–protein bioconjugates debrided from the sensor surface may be immunogenic or allergenic (Lee *et al* 2001, 2004, 2010, Lee 2010). More mechanically robust films may therefore be desirable in clinically deployed bio/immunoFETs.

We previously detected concentrations of the protein analyte b-MIG similar to those that native MIG attains in highly inflamed tissue, in a physiological osmolarity buffer with an AlGaN/GaN bioHFET (Gupta *et al* 2008). That bioHFET was not sufficiently sensitive to detect MIG across its reported clinical concentration range (normal to inflamed tissue levels), and we hypothesized that clearer understanding of the polymer/analyte receptor interfacial film structure of the HFET could help us design sensors with better sensitivity. The hypothesis seems to be substantially valid: a more optimal interface has produced a device which, despite little modification of the HFET architecture *per se*, is much more sensitive than was its predecessors (Gupta *et al* 2010, Nicholson *et al* 2010). In characterizing the sensing surface and the interfacial polymer film, we found that, contrary to prior assumptions (Bhushan *et al* 2009), using the oxidation protocol used in Gupta *et al* (2008), oxides of gallium, not aluminium, were more prevalent at the HFET surface (Wen *et al* 2010). Sensor surface properties, or arguably, underlying substrate electrical properties, can substantially influence the ability of the surface to support silane derivatization (Arranz *et al* 2008, for a GaN surface, and Wen *et al* 2010). Deposition protocols also influence morphology of silane films (Bhushan *et al* 2009), but the specific silane compound used to build films can have a profound effect on film parameters. Congruent with our findings of networked 3-APTES films deposited on alumina and silica using solution deposition methods, (Bhushan 2009, figures 3 and 4) and with networked 3-APTES films deposited on n-type Gan (Arranz *et al* 2008), we present AR-XPS data suggesting that 3-APTES films are also more disordered and networked than are 3-APTES films on AlGaN (Wu *et al* 2010). The differential protein binding properties (binding kinetics and quantity) of our 3-APTES and APDMES films on AlGaN also suggest the former to be networked, and the latter a monolayer, or nearly so. Lesser mechanical robustness of 3-APTES than APDMES films on multiple metal oxides can be rationalized from the extent of silane–silane cross-linking and disparate average numbers of silane linkages to the oxide per monomer in the two types of films. *In toto*, the observations led us to propose models of protein distribution (streptavidin and b-MIG) in 3-APTES and APDMES on AlGaN that are testable, and may help rationalize sensor behaviour.

Our analysis leads us to suspect that lack of appreciation of primacy of the interfacial structure in the performance characteristics of FET protein sensors may have led to the historically variable, and frequently poor, performance of planar protein sensing bio/immunoFETs with various polymer/protein interfaces (Bergveld 1991, Schoning and Poghossian 2002). The lack of clear and consistent protein sensing results may have fuelled the dismissal of planar immunoFETs as biosensors (Bergveld 1991, Schoning and Poghossian 2006), that we (Shapiro *et al* 2007, Eteshola *et al* 2008, Gupta *et al* 2008, Bhushan 2010) and others (Lud *et al* 2006, Baumgartner *et al* 2009, Estrela *et al* 2010) argue to have been premature. Interfacial design is emerging as a potentially critical parameter in design and realization of immunoFETs and other FETs that sense the charges or electrical fields of protein analytes directly.

Acknowledgments

This work was supported in part by award GRT00015533 from the National Science Foundation, awards from The Program for Homeland Security of the Ohio State University and awards from the Institute for Materials Research of the Ohio State University.

References

Arranz A, Palacio C, Garcia-Fresnadillo D, Orellana G, Navarro A and Munoz E 2008 Influence of surface hydroxylation on 3-aminopropyltriethoxysilane growth mode during chemical functionalization of GaN surfaces: an angle-resolved x-ray photoelectron spectroscopy study *Langmuir* **24** 8667–771

Baumgartner O E, Orio R, Wagner P J, Windbacher T and Selberherr S 2009 *VISTA Status Report* Institute for Microelectronics, Vienna, Austria

Baur B, Steinhoff G, Hernando J, Purrucker O, Tanaka M, Nickel B, Stutzmann M and Eickhoff M 2005 Chemical functionalization of GaN and AlN surfaces *Appl. Phys. Lett.* **87** 263901

Bergveld P 1991 A critical evaluation of direct electrical protein detection methods *Biosensors Bioelectron.* **6** 55–72

Bergveld P 1996 The future of biosensors *Sensors Actuators* A **56** 65

Bergveld P 2003 Thirty years of ISFETology: what happened in the past 30 years and what may happen in the next 30 years *Sensors Actuators* B **88** 1–20

Bhushan B *et al* 2005 Morphology and adhesion of biomolecules on silicon based surfaces *Acta Biomater.* **1** 327–41

Bhushan B *et al* 2006 Nanoscale adhesion, friction and wear studies of biomolecules on silicon based surfaces *Acta Biomater.* **2** 39–49

Bhushan B *et al* 2009 Nanoscale adhesion, friction and wear studies of biomolecules on silane polymer-coated silica and alumina-based surfaces *J. R. Soc. Interface* **6** 719–33

Bhushan B 2010 *Springer Handbook of Nanotechnology* 3rd edn (Heidelberg: Springer)

Cui Y, Wei Q, Park H and Lieber C 2001 Nanowire nanosensors for highly sensitive and selective detection of biological and chemical species *Science* **293** 1289–92

Estrela P *et al* 2010 Label-free sub-picomolar protein detection with field-effect transistors *Anal. Chem.* **82** 3531–6

Eteshola E *et al* 2008 Engineering functional protein interfaces for immunologically modified field effect transistor (ImmunoFET) by molecular genetic means *J. R. Soc. Interface* **5** 123–7

Fahmy N M *et al* 2003 Chemokine and chemokine receptor gene expression indicates acute rejection of human cardiac transplants*Transplantation* **75** 72–8

Gupta S, Elias M, Wen X, Shapiro J, Brillson L, Lu W and Lee S C 2008 Detection of clinically relevant levels of protein analyte under physiologic buffer using planar field effect transistors *Biosensors Bioelectron.* **24** 505

Gupta S, Wen X, Casal P, Nicholson T R III, Wu H-H, Brillson L J, Lu W and Lee S C 2010 The effect of interface modification on bioFET sensitivity, submitted

Han Y, Mayer D, Offenhauser A and Ingebrandt S 2006 Surface activation of thin silicon oxides by wet cleaning and silanization *Thin Solid Films* **510** 175–80
Israelachvili J N 1991 *Intermolecular and Surface Forces* 2nd edn (London: Academic)
Kallury K M R, Macdonald P M and Thompson M 1994 Effect of surface water and base catalysis on the silanization of silica by (aminopropyl)alkoxysilanes studied by x-ray photoelectron spectroscopy and 13C cross-polarization/magic angle spinning nuclear magnetic resonance *Langmuir* **10** 492–9
Kang B S *et al* 2005 Electrical detection of immobilized proteins with ungated AlGaN/GaN high-electron-mobility transistors *Appl. Phys. Lett.* **87** 023508-3
Kang B S *et al* 2007 Prostate specific antigen detection using AlGaN/GaN high electron mobility transistors *Appl. Phys. Lett.* **91** 112106
Lee S C *et al* 2005 Protein binding on thermally grown silicon dioxide *J. Vac. Sci. Technol.* B **23** 1856–65
Lee S C *et al* 2001 Recognition properties of antibodies to PAMAM dendrimers and their use in immune detection of dendrimers *Biomed. Microdevices* **3** 53–9
Lee S C *et al* 2004 Biochemical and immunological properties of cytokines conjugated to dendritic polymers *Biomed. Microdevices* **6** 191–202
Lee S C 2010 Implications of available design space for identification of non-immunogenic protein therapeutics *Biomed. Microdevices* **12** 283–6
Lee Y, Ferrari G and Lee S C 2010 Estimating design space available for polyepitopes through consideration of major histocompatibility complex binding motifs *Biomed. Microdevices* **12** 207–22
Liao Y-S, Benya P D and McKellop H A 1999 Effect of protein lubrication on the wear properties of materials for prosthetic joints *J. Biomed. Mater. Res.* **48** 465–73
Lide D R 2003 *CRC Handbook of Chemistry and Physics* 83rd edn (Boca Raton, FL: CRC Press)
Lud S Q *et al* 2006 Field effect of screened charges: electrical detection of peptides and proteins by a thin-film resistor *ChemPhysChem* **7** 379–84
Muira M *et al* 2001 Monokine induced by Inf g is a dominant factor directing T-cells into murine cardiacallografts during acute rejection *J. Immunol.* **167** 3494–504
Muira M *et al* 2003 Neutralization of monokine induced by interferon-g during the early posttranslation period prevents development of chronic allograft vasculopathy and graft fibrosis *Transplant. Proceed.* **35** 875–7
Nair P R and Alam M A 2008 Screening-limited response of nanobiosensors *Nano Lett.* **8** 1281–5
Nicholson T R III *et al* 2010 Optimization of nanobiotechnological devices illustrated by partial optimization of a protein sensing field effect transistor *J. Nanoeng. Nanosyst.* at press
Ogawa N *et al* 2002 Involvement of the interferon-gamma-induced t cell-attracting chemokines, interferon gamma inducible 10 kd protein (CXCL10 and monokine induced by interferon-gamma (CXCL9), in the salivary gland lesions of patients with Sjorgens Syndrome *Arthritis Rheumatism* **46** 2730–41
Reiners J *et al* Mig, IP-10 and CXCR3 gene expression is predictive for the individual response of children with chronic allograft nephropathy to mycophenolate moftiel *Transplant. Proceed.* **34** 2217–8
Romagnani P *et al* 2002 Expression of IP-10/CXCL10 and MIG/CXCL9 in the thyroid and increased levels of IP-10 CXCL10 in the serum of patients with recent-onset Graves' disease *Am. J. Pathol.* **161** 195–206
Ruschpler P *et al* 2003 High CXCR3 expression in synovial mast cells associated with CXCL9 and CXCL10 expression in inflammatory synovial tissues with rheumatoid arthritis *Arthritis Res. Ther.* **5** R241–R252
Scholes S C, Unsworth A, Hall R M and Scott R 2000 The effects of material combination and lubricant on the friction of total hip prostheses *Wear* **241** 209–13
Schöning M J and Poghossian A 2002 Recent advances in biologically sensitive field-effect transistors (BioFETs) *The Analyst* **127** 1137
Schöning M J and Poghossian A 2006 Bio FEDs (field-effect devices): state-of-the-art and new directions *Electroanalysis* **18** 1893–900
Shackelford J S and Alexander W 2001 *CRC Materials Science and Engineering Handbook* 2nd edn (Boca Raton, FL: CRC Press)
Shapiro J P, S K Gupta, Elias M A, Wen X, Eteshola X, Brillson L, Lu W and Lee S C 2007 Challenges in optimization of nanobiotechnological devices illustrated by partial optimization of a protein biosensor *Proc. 2nd Int. Congress of Nanobiotechology & Nanomedicine*
Takahata Y *et al* 2003 Detection of interferon-gamma-inducible chemokines in human milk *Acta Paediatr.* **92** 659–65
Teixeira A L Jr *et al* 2004 Increased serum concentrations of monokine induced by interferongamma/CXCL9 and interferon-gamma-inducible protein 10/CXCL-10 in Sydenham's chorea patients *J. Neuroimmunol.* **150** 157–62
Wang A, Essner A and Schmidig G 2004 The effects of lubricant composition on in vitro wear testing of polymeric acetabular components *J. Biomed. Mater. Res.* B **68** 45–52
Wang D, Sai J and Richmond A 2003 Cell surface heparan sulfate participates in CXCL1-induced signaling *Biochemistry* **42** 1071–7
Watts J and Wolstenholme J 2003 *An Introduction to Surface Analysis by XPS and AES* 2nd edn (New York: Wiley)
Weber P C, Ohlendorf D H, Wendoloski J J and Salemme F R 1989 Structural origins of high-affinity biotin binding to streptavidin *Science* **243** 85–8
Wen X S, Schuette M L, Gupta S, Lee S C and Lu W 2010 Improved sensitivity of AlGaN/GaN field effect transistor biosensors by optimized surface functionalization *IEEE Sensors J.* at press
Wu H-H, Rutkowski M, Gupta S, Wen X, Nicholson T R III, Lu W and Brillson L J 2010 Angle-resolved x-ray photoemission spectroscopy of self-assembled protein monolayers on AlGaN/GaN immuno-modified field effect transistors *J. Vac. Sci. Technol.* B submitted
Youtsey C, Adesida I and Bulman G 1997 Highly anisotropic photoenhanced wet etching of n-type GaN *Appl. Phys. Lett.* **71** 2151–3
Zhao D *et al* 2002 Differential expression of the IFN-g inducible CXCR3-binding chemokines, IFN-inducible protein 10, monokine induced by IFN and IFN-inducible T-cell a chemoattractant in human cardiac allograft vasculopathy *J. Immunol.* **169** 1556–60
Zheng G, Patolsky F, Cui Y, Wang W and Lieber C 2005 Multiplexed electrical detection of cancer markers with nanowire sensor arrays *Nature Biotechnol.* **23** 1294–301